Madhani, Jehangir T. and Young, Joe and Kelson, Neil A. and Brown, Richard J. (2009) *A novel method to capture and analyze flow in a gross pollutant trap using image-based vector visualization.* Water, Air, & Soil Pollution : Focus.

A novel method to capture and analyze flow in a gross pollutant trap using image-based vector visualization

Jehangir T. Madhani[1,*], Joseph Young[2], Neil A. Kelson[2] and Richard J. Brown[1]

[1]*School of Engineering Systems, Queensland University of Technology, QLD 4001, Australia.*

[2]*HPC & Research Support Group, Queensland University of Technology, Brisbane, QLD 4001, Australia.*

([*]author for correspondence: j.madhani@qut.edu.au; tel: 61 7 31389127; fax: 61 7 31381170)

Abstract

A novel method is developed to capture and analyse several experimental flow regimes through a gross pollutant trap (GPT) with fully and partially blocked screens. Typical flow conditions and screen blockages are based on findings from field investigations that show a high content of organic matter in urban areas. Fluid motion of neutral buoyant particles is tracked using a high-speed camera and particle image velocimetry (PIV) software. The recorded fluid motion is visualized through an image based, line integral convolution (LIC) algorithm, generally suitable for large computational fluid dynamics (CFD) datasets. The LIC method, a dense representation of streamlines, is found to be superior to the point-based flow visualization (e.g., hedgehog or arrow plots) in highlighting main flow features that are important for understanding litter capture and retention in the GPT. Detailed comparisons are made between the flow regimes, and the results are compared with CFD data previously obtained for fully blocked screens. The LIC technique is a useful tool in identifying flow structures in the GPT and areas that are subjected to abnormalities difficult to detect by conventional methods. The novel method is found to be useful both in the laboratory and in the field, with little preparation and cost. The enhancements and pitfalls of the LIC technique along with the experimentally captured flow field are presented and discussed.

Keywords: *Line integral convolution (LIC), gross pollutant trap (GPT), litter, flow visualisations*

Abbreviations: GPT, gross pollutant trap; CFD, computational fluid dynamics; LIC, line integral convolution; ADV, Acoustic Doppler Velocimeter; PIV, particle image velocimetry.

1. Introduction

Stormwater is surface flow runoff from urban areas discharging into receiving waterways. The pollutants collected by stormwater along the path of urban runoff threaten the aquatic and terrestrial ecosystem (Borchardt and Sperling, 1997). This has led to
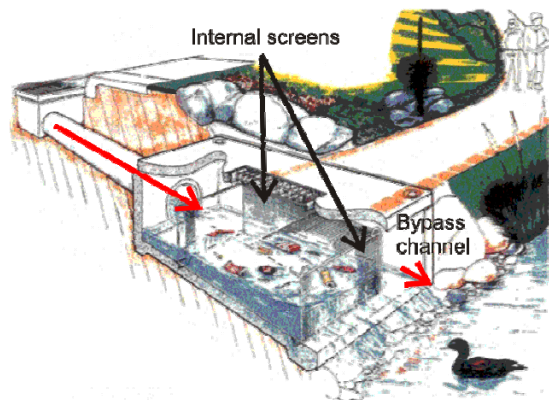

Fig. 1: GPT – LitterBank *in situ*

the development of stormwater quality improvement devices (SQIDs) to efficiently trap gross and fine pollutants, for historical overview see Madhani et al. (2009a). Gross pollutants traps (GPTs) are a class of SQID designed to trap pollutants dimensionally greater than 5 mm. Gross pollutants are defined as visible waste such as litter and organic matter. A linear screening GPT, LitterBank, was recently developed by C-M Concrete Pty Ltd. It uses retaining screens to collect gross pollutants prior to the release of the stormwater into natural waterways (Fig. 1). Currently there are 20 LitterBanks operating at strategic stormwater locations throughout Queensland, Australia.

A review of the literature indicates that field monitoring and physical modelling of GPTs with either real or simulated pollutants are well documented, but the hydrodynamic details of velocity vector fields are limited more so in terms of the flow domain coverage (Madhani et al. 2009b). Engineering flow structures provide valuable insights into pollutant capture and retention characteristics due to regions of flow recirculation and critical (high and low) velocities. These flow features can cause erosion, containment and/or mobilization of pollutants

(Harwood 2002). The deposition pattern of particles has been shown to be directly related to the flow pattern observed at the water surface (Stovin et al. 1999). Although computational fluid dynamic simulation is an alternative, modelling uncertainties exist and validation is often incomplete due to lack of experimental data.

Hydrodynamic characteristics have been investigated previously in an experimental rig consisting of a pipe inlet and a scale-model GPT (Madhani et al. 2009b). Velocity profile measurements were taken at a fixed depth throughout the trap with an Acoustic Doppler Velocimeter (ADV). Full domain flow coverage is extremely laborious using the ADV technique. Furthermore, fluid velocities closer to the free surface are not captured since the ADV probe requires to be submerged for proper operations (Madhani et al. 2009b). Consequentially, visual observations of surface flow features within the GPT had to be taken due to their likely importance for understanding litter capture and retention.

Advancement of modern optical and digital processing methods has led to capabilities in capturing extensive flow field data rather than single point ADV measurements in experimental fluid mechanics. Several authors have used a similar PIV setup to investigate velocity flow fields in other fluidic devices (Kandikar et al., 2009; Li and Wang, 2009; Hossain et al., 2007).

In this experiment, a method is developed to analyze several flow regimes through an experimental rig consisting of a rectangular channel inlet and a scale-model GPT to study pollutant-free flow in a trap. Typical flow conditions and blocked screens are based on findings from field investigations that show a high content of

organic matter in urban areas. Fluid motion of neutral buoyant particles is tracked using a high-speed camera and particle image velocimetry (PIV) software. The recorded fluid motion is visualized through an image based, line integral convolution (LIC) algorithm.

Line integral convolution (LIC) is widely used in computational fluid dynamic visualization for highlighting both global and local flow features. Direct flow visualization (e.g., hedgehog or arrow plots) may be intuitive but impractical for large 2D or 3D datasets due to visual clutter caused by the dense rendering of arrow glyphs. Regions of high velocity where the arrow glyphs become long can also obscure the clarity of hedgehog visualization hence the smaller flow details can be missed. The LIC method, a dense representation of streamlines, is superior to the point-based (direct) flow visualization in providing full spatial flow domain coverage, but the use of streamlines to investigate a whole flow region is difficult since the coverage is highly dependent on the streamline seed points. Kao and Shen (1998) found that LIC images were superior to streamlines in revealing separation and reattachment lines on a model aircraft. However, techniques have been developed that employ streamline-seeding strategies which produce families of streamlines that cover more of the flow domain (Turk and Banks 1996). Further work is required to test this method on the experimental dataset.

In this investigation, the experimental flow dataset is sufficiently large for a LIC technique to be used. An image based, line integral convolution (LIC) algorithm is used to highlight the flow features that are important for understanding litter capture and retention in the GPT. Detailed comparisons are made of the flow regimes and with previously obtained 2D CFD data (Madhani et al. 2009b). The

LIC technique with its enhancements and pitfalls, along with the captured flow, are presented and discussed in this paper. Most proprietary GPTs are designed and constructed based on criteria which are often unique to a specific treatment system. Such GPTs will have specific flow structures resulting from their unique patented characteristics that require their own testing program (Rushton et al. 2007). This method is convenient and useful in the preliminary investigation of the flow structure within the GPT, particularly to establish regions of interest.

While acknowledging some uncertainties in the two-dimensional depth coverage, this simplified approach permits the added benefit of investigating a range of flow regimes, which otherwise would be labour intensive.

To the best of the authors' knowledge, work relating to (a) dense, texture-based vector field visualization and (b) flows in GPTs similar to the one studied is limited. This is the first time that texture-based vector field techniques have been used to visualize experimentally collected vector fields.

2. Field study

Ian Cordery (2005) describes the change in the constitution of gross pollutants in Australian cities over the last thirty years. In the 1970s, street litter was composed of human derived waste and organic matter in equally quantities. The current trend however exhibits a larger proportion of organic matter. Australian data on gross pollutants first became available in 1986 (Nielsen and Carleton 1989). An extensive literature review on gross pollutants is conducted from this date and confirms the growing problem of organic matter. For example, volumetric data collected by Nielsen and Carleton (1989) for the Sydney region shows that

organic matter varied from 22% to 50%. A decade later for the same location, organic matter was found to comprise almost 80% with little variation (Van Drie 2002).

In Melbourne, Allison and Chiew (1995) correlated the composition of gross pollutants in terms of mass with urban land usage. In the two extremes cases, organic matter from light industrial and residential sites varied from 36% to 85% respectively. In mixed commercial

Fig. 2: Clippings from grass verge collected at a stormwater drain at Park Road, South Brisbane (2008)

and residential areas, organic matter was approximately 65%. Allison et al. (2000) showed volume and mass classifications to be similar and concluded that, irrespective of the methods used to analyse the concentrations of the gross pollutant components, the derived values were usually between 70 and 90 percent for organic matter and between 10 and 30 percent for human derived litter in mixed commercial, industrial and residential urban centres. A higher trend has been reported for Hobart (Chrispijn 2004).

Mass data collected from the outer suburbs of Brisbane in mainly residential areas (70–98%) by Brisbane City Council (2004) and Greenway et al. (2005) reveal a similar amount of organic matter (93%). Here, most of the collected gross pollutant data relates to the contents of GPTs.

The high level of organic matter in stormwater is a cause for concern. Observations during the field study show that grass clippings are often left to accumulate along the roadside (Fig. 2). Furthermore, gross pollutants are also a transport mechanism for finer stormwater pollutants. Organic waste causes blockages to stormwater drains and contributes to the nutrients that enter waterways, creating oxygen-depleting substances that are detrimental to the aquatic habitat. Since city planners and architects are promoting the concepts of green walls and roofs in urban centres, buildings cladded with vegetation will increase the nutrient load in waterways.

In this field survey, data are collected from the Brisbane central business district (CBD), South Brisbane, and the Burleigh Heads CBD. These sites are chosen to reflect a range of residential and commercial urban activities. The data are collected over a two-year period. Photographs and field
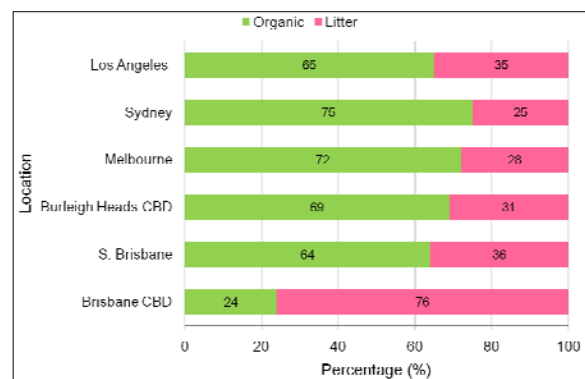

Fig. 3: Results of the litter field survey taken from 2006 to 2008. Comparison of gross pollutant (organic & litter) data are made with data collected from Sydney (Van Drie 2002), Melbourne (Lewis 2002) and Los Angeles (Quasebarth et al. 2001; Lippner et al. 2000)

notes are taken for analysis. The concentration of gross pollutants is determined by mapping the surface of the littered area on the photograph and using an area ratio method to derive a percentage value. In cases where organic matter and litter were well mixed and difficult to segregate, the waste components were visually approximated.

The results of the field survey consist of data collected from 75 stormwater drains and reveal a high percentage of organic matter (60–70%) in all areas, with the exception of the Brisbane CBD, where human derived litter such as fast-food packaging, plastic, and beverage containers predominates. The results are on a par with findings from other cities (Fig. 3).

3. Physical Modelling

Field monitoring of GPTs in Brisbane indicates that during wet weather a wide range of inlet, outflow and other operating conditions occur. For example, the extent and duration of rainfall influences the flow rate entering the trap. The tidal or flood levels of the downstream receiving waterways will determine the outflow level in the GPT (Fig. 4a). Due to infrequent cleaning, the retaining screens are often found to be blocked with organic matter (Figs 4b and 4c). Partially or fully blocked screens can radically change the litter retention characteristics and flow structure

(a) High tide downstream causes flooding in the GPT LitterBank.

(b) Front view of a partially blocked screen with organic matter from incoming stormwater.

(c) Fully blocked screens.

Fig 4: Field surveys showing the GPT LitterBank with (a) high, and (b) low water tidal levels, partially and (c) fully blocked screens.

within the GPT, leading, for example, to large recirculating flow patterns within the trap area accompanied by hydraulic short circuiting (Thackston et al. 1987) where the preferred outflow path is via the bypass channel. In this work, fully and partially blocked screens in the GPT are modelled with solid and perforated internal walls respectively.

Depending on the operating conditions, the possible flow regimes inside the GPT can range from turbulent time-dependent free surface flows to more steady-state conditions, and this presents significant challenges for experimental or numerical studies aimed at understanding the flow and litter retention characteristics of the trap (Madhani et al. 2009b). To facilitate their study of steady-state flow conditions, Madhani et al. (2009b) developed an experimental approach using a downstream weir arrangement to control the nature of the flow and the variation in free surface height in the GPT. The weir height can also replicate the elevated outflow water levels into the receiving waterway due to rainfall or storm events. The experimental approach resulted in a matrix of flow regimes appropriate for a range of low to high operating GPTs (see Table 2 below).

4. Experimental Method

The experimental rig (50% scale model GPT) is placed in a square-section (19 m, 0.6 m wide, 0.6 m deep) tilting flume at the QUT hydraulic laboratory. The flume inclination is set to horizontal and a constant flow rate is established via controller settings on the centrifugal pumps that circulate water from underground storage tanks into the flume. Flow rate readings are checked with periodical measurements in the collection tank at the flume outlet. Flow into the scale model GPT is through a horizontal 1.8 m length inlet rectangular channel with an

internal width of 146 mm. To promote smooth upstream flow conditions, three mesh screens 1 m apart are inserted at the upstream end of the flume.

Table 1 shows materials used to replace normal screens in the GPT to represent typical blockages found in field studies.

Table 1: Material used in replaced of normal screens in the GPT to represent percentage of blocked screens.

Material	Blockages (%)
Perspex solid walls	100
Perforated screens (3 mm holes)	68
5 mm mesh	33
No screens	0

The percentage blockages are based on the amount of material obstructing the flow path. To study pollutant-free flow in a trap with fully blocked screens (i.e. 100% blockages) the GPT model is fitted with solid internal walls. A perforated screen with 3 mm circular holes represents 68% blockages while a 5 mm rectangular mesh screen represents 33% blockages.

The measurement runs for the matrix of flow rates based on field investigations are shown in Table 2. Flow rates of 1.3 l/s and 3.9 l/s are set with corresponding weir heights of 0.1 m and 0.3 m respectively, at the end of the flume terminus raceway. Some variations in flow conditions (± 10%) during the course of the experiments are unavoidable since the constant head tank is not fitted to the flume. Further details on the experimental setup are given by Madhani et al. (2009b). For higher flow regimes, the weir height is set at the floor level of the raceway (zero).

Table 2: Experimental setup of flow regimes through a GPT with designated blocked screen runs

Flow regime	Weir height (m)	Inlet Velocity (m/s)	Flow Rate (L/s)	Water depth in Trap (m)	Screen blockages %		
					100	68	33
Low	0.108	0.09	1.3	0.1	R1	R3	R5
↑	0.286	0.09	3.9	0.3	R2	R4	R6
↓	0	0.39	6.13	0.1	R7	R9	R11
High	0	2.14	35	0.3	R8	R10	R12

Flow structures within the GPT are obtained by tracking fluid particle motion with a high-speed camera (X-Stream [TM] XS-4), image acquisition (X-Vision version 1.13.05) and processing using PIV software (IDT 2005a and b) suite (proVision-XS version 3.08.30). The PIV system is supplied by Integrated Design Tools Inc. (IDT). The camera is connected to a PC Pentium 4Mhz. The camera has a ¼-inch format and is fitted with an 8 mm focal length CCTV lens manufactured by Computar (M0814-MP). The distance from the lens to the GPT floor is 1.5 m and the vertical view for the maximum water depth coverage is given by: $f = v\dfrac{D}{V}$, where f is the focal length, v is the factor dependent on the camera format, D is the distance from lens to object and V is the vertical (depth) view of field. A vertical view of field of at least 0.5 m is thus obtained for a given factor $v = 2.7$. Since the maximum water depth is 0.3 m, adequate focus is achieved for all experimental runs.

The camera is mounted on a tripod and calibrated on a 40 mm gridded paper position inside the scale model GPT (IDT, 2005b). Illumination of the seeded particles is achieved by positioning 1000-watt portable halogen floodlights above the GPT and at the sides. An attempt is made to direct the light in a confined, almost planar area of the intake withdrawal field using slotted sheet metal to enhance the recorded image quality. A polarized lens is also used to reduce the reflection of light from the water surface and internal walls.

The fluid motion of the particles is tracked within the GPT using neutral buoyant particle seeding (20–50 μm), which is introduced into the upstream inlet flow via

a feeding system. To avoid clumping of the particles, the outlet seeding tube has to be positioned just below the water surface, and each run is repeated several times. The acquisition rate varies between 30 to 90 Hz depending on the flow rate.

The experimental video recordings from the acquisition software (X-Vision) are exported into the PIV image processing program (proVision-XS). A high resolution grid is constructed which covers the entire flow domain within the GPT to generate the x and y coordinates. The PIV program uses tracking algorithms to produce two-dimensional velocity vector fields in terms of the x and y coordinates. The non-uniform velocity data (x, y coordinates and point velocities Ux, Uy) are exported into a text file (filename.plt); typically, each file comprises 5000 data points.

5. The Line Integral Convolution (LIC)

5.1 The line integral convolution method

We begin by describing a vector field and its directional structure in order to define streamlines (Stalling and Hege 1995). Let v be a vector field, defined by $v : \Re^2 \to \Re^2, x^2 \mapsto v(x)$ and let $\sigma(u)$ be an integral path of v, such that:

$$\frac{d}{du}\sigma(u) = v(\sigma(u)) \qquad (1)$$

By definition, the tangent vector of $\sigma(u)$ coincides with v and thus $\sigma(u)$ can be used to depict the orientation of v. For our purposes, it is useful to re-parameterize $\sigma(u)$ by its arc-length s. We note that $\frac{ds}{du} = |v(\sigma(u))|$, and hence

$$\frac{d}{ds}\sigma(s) = \frac{d\sigma}{du}\frac{du}{ds} = \frac{v}{|v|} \equiv f(\sigma(s)) \qquad (2)$$

In other words, by normalizing v, we can calculate σ as a function of its arc-length s. This re-parameterization is only valid when $|v| \neq 0$, i.e., for non-degenerate curves σ. A streamline through x can be calculated by solving the ordinary differential equation (1).

We describe the LIC method where the flow domain is represented by dense streamlines. This method has received considerable interest because global and local flow details are visualized throughout the spatial domain. The generation of LIC based textures or images of a vector field v can be described as the blurring of a white-noise input texture I along the streamlines of v. This method was originally developed by Cabral and Leedom (1993) and the modification proposed by Stalling and Hege (1995) is currently used here. Given a streamline σ, the LIC technique calculates the intensity $O(x_0)$ for a pixel located at x_0 as follows:

$$O(x_0) = \int_{x_0-l}^{x_0+l} k(s) I(\sigma(s)) ds \qquad (3)$$

Here, I denotes a random noise input texture image (we use a white-noise image) and $k(s)$ is

Experimental video recordings of seeded flow in a GPT

2D PIV data
(x, y, U_x, U_y)

Data Preparation

Construct smooth interpolation profiles F_1 and F_2 through U_x, U_y (TRIPACK/ SRFPACK)

Map data to regular & uniform grid G_{xy} (SRFPACK)

New dataset on a regular and uniform grid G_{xy}, V_x, V_y

LIC Algorithm

Initialise output image matrix, O and generate a white noise image matrix texture, I.

For each pixel, perform LIC algorithm

Output image O
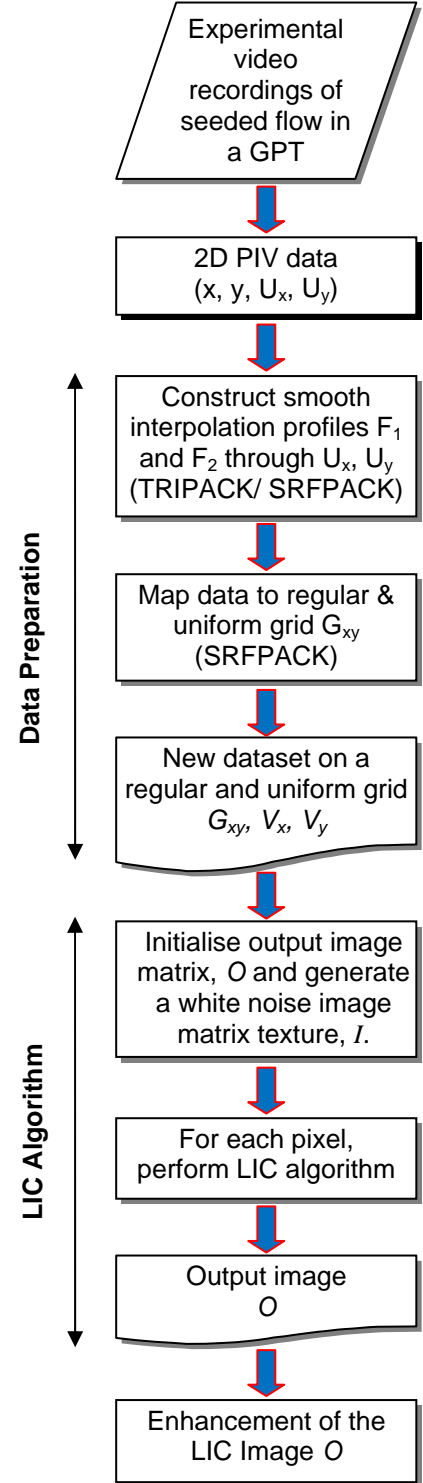
Enhancement of the LIC Image O

Fig. 5: Overall view of the steps for producing the LIC image

a smoothing one-dimensional filter kernel; l is the length of both the forward and backward streamlines; O is the output (LIC) image. We use a box filter where $k(s)$ = 1, $x_0\text{-}l \leq s \leq x_0\text{-}l$ and 0 otherwise. The convolution integral (3) is discretized by taking L steps of length h along both forward and backward streamlines seeded from x_0. This leads to the following:

$$O(x_0) = \frac{1}{2L+1} \sum_{i=-L}^{L} k(x_i)I(x_i), \ x_i = \sigma(ih) \quad (4)$$

Our method for generating LIC images of the vector field v has two parts: an interpolation process followed by the application of the LIC algorithm as described by Stalling and Hege (1995). The interpolation process allows the vector field v to be mapped onto a uniform Cartesian grid G_{xy} that is amenable to the LIC algorithm. Each point of the uniform grid corresponds to a pixel of the output LIC image O. In this case, the experimental process generates the vector field v with velocities located at irregularly scattered points. An overview of the steps performed in creating a LIC image from a scattered set of experimentally generated sampled velocities is shown in Fig. 5.

The interpolation process is implemented to use two-dimensional cubic spline interpolations (Renka and Cline 1992), which are applied successively to the irregularly spaced stream (U_x) and crosswise (U_y) velocities to generate two surfaces F_x and F_y respectively. SRFPACK (ACM, 1996) is a fast, robust code for the interpolation of scattered data; it is used to carry out the interpolations. It is a FORTRAN 77-based code that allows for the triangulation and calculation of a smooth interpolant through scattered data points, optionally defined within a non-convex domain i.e., arbitrary shaped boundaries. The interpolation consists of a set of three cubic surface patches, defined on each triangular element of a

Delaunay triangulation of the scattered data. (Note, each surface patch is defined on a sub-triangle obtained by joining the vertices to the triangle's barycentre). Using the interpolating surfaces F_x and F_y, the stream and crosswise velocity components are calculated on the regular uniform grid G_{xy}, suitable for the LIC algorithm. We denote the interpolated vector field lying on G_{xy} as $V = [V_x, V_y]^T$.

We have typically generated LIC images of 600 x 800 pixels. The method begins with the initialization of the output image matrix O to zeros, the generation a random white-noise input image I and the normalization the vector field velocities $V = [V_x, V_y]^T$ to unity. If $|[V_x, V_y]^T|$ is near zero, $[V_x, V_y]^T$ is set to $[0,0]^T$. The normalization enables the convolution integral (3) to be approximated using (4) by sampling the input image I at evenly spaced points x_i along σ. The pseudo-code below describes the LIC algorithm:

STEP 1: Initialization

Initialize the output image O to zeros, generate a random white-noise input image I.

Normalize the vector field $V = (V_x, V_y)^T$ to unity – if a zero (or near zero) vector is encountered,
   set the vector at this location to $[0,0]^T$.

STEP 2: Streamline generation and convolution

For each pixel p_{ij} in the output image O

   Generate a forward streamline S_f of length L, seeded at pixel p_{ij} (see Note 1 below)

   Generate a backwards streamline S_b of length L, seeded at pixel p_{ij} (see Note 1 below)

   Construct $S = S_f \ U \ S_b$

   Set $Sum = 0$ (accumulates the sum of all pixel values lying on the streamline S)

   For each point S_p on the streamline S

      determine the value p_v of the underlying pixel p of the white noise image I - we
         choose the closest pixel p to S_p

      $Sum = Sum + p_v$

End

Add *Sum /(Number of pixels on the streamline S)* to pixel p_{ij} of the output image O

End

STEP 3: Store or display output image O

It should be noted that:

1. If the streamlines S_f or S_b exit the domain or encounter a zero velocity vector, both streamline calculations are terminated after $K < L$ steps.

2. Along the streamline S at evenly spaced points x_i, $i=1,…, K \leq L$, not all of the points x_i will lie on the nodes of the uniform grid G. In this case, we use bilinear interpolation across the rectangular cell containing x_i to determine the underlying velocity vector.

3. We use an accurate fourth-order Runge-Kutta integrator (RK4), with a step size $h = 0.5$, to calculate the points x_i lying on the streamline S. The RK4 method is a fourth-order method.

4. With the integration step size set to $h = 0.5$, it is guaranteed that all pixels lying along the streamline S will be sampled, since pixels are separated by a unit distance.

5.2 Enhancement of the LIC Image *O*

The LIC algorithm repeatedly applies a low-frequency filter (see equation (4)) to the noise input image I. This blurs the image I along the input vector field V. Inherently, the low-pass filter averages the pixel intensities and hence image contrast is lost. One or more image processing techniques are usually applied to the LIC image O to reduce blurring and restore the image contrast. Typical enhancements include high frequency filtering to sharpen the image and

histogram equalization to restore contrast. Our implementation allows any general 3x3 image filter to be applied to the LIC image along with histogram equalization. We have experimented with a range of high-pass filters in combination with histogram equalizations and our experience to date indicates that the application of the histogram equalization alone sufficiently enhances image quality. Hence, LIC images included at the end of this paper have been post-processed with histogram equalization.

In the following section, we discuss the application of the LIC algorithm to the experimental PIV data sets.

6. Results and Discussion

We commence the discussion by choosing an experimental dataset to compare the captured vector field using vector plots with LIC images. Figs 6a and 6b show a captured flow field for dataset R3, using a camera and a PIV software. Fig. 6a, a sample of a single frame shot, shows the seeded flow in the GPT with neutrally buoyant particles. Fig 6b shows an average statistical image processed PIV vector plot. The vector plot in Fig. 6b is improved by importing the data into Matlab (version 2008a), and the resulting image is depicted in Fig. 6c. An attempt to visualise the data using an open source visualisation package (OpenDx) is also made with no significant improvement in comparison to Fig 6c. However, the application of LIC to the same dataset clearly shows superior flow domain coverage particularly for regions of low velocities (R3 in Figs 7 and 8). The flow structures in the R3 dataset are clear and well defined, indicating sufficient data

points were collected. The results demonstrate the potential of the method developed for the purpose of capturing and analysing flow in a GPT.

To identify flow structures in the LIC images (Figs 7 and 8), comparisons are made with previous work of the same experimental setup (Madhani et al. 2009b). Here, the main flow structures in a GPT with fully blocked screens for run R1 (Table 2) have been theoretically (CFD) and experimentally identified. The CFD flow field is shown in the form of streamlines and a vector plot in Figs 9a and 9b respectively. The main flow structures consist of the deflection of the entry jet into the bypass channel, and the existence of a large recirculation flow within the retention area of the trap (Fig. 9a). Smaller near-wall features were also observed (Fig. 9a), such as secondary recirculation (zone 4), flow separation (zone 5) and low-velocity corner eddies
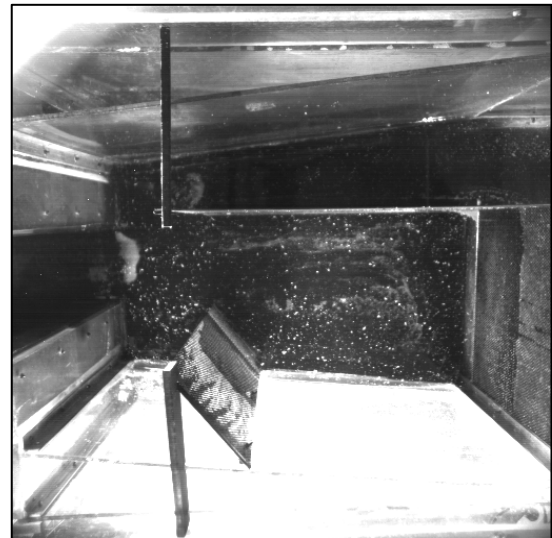
(a) R3
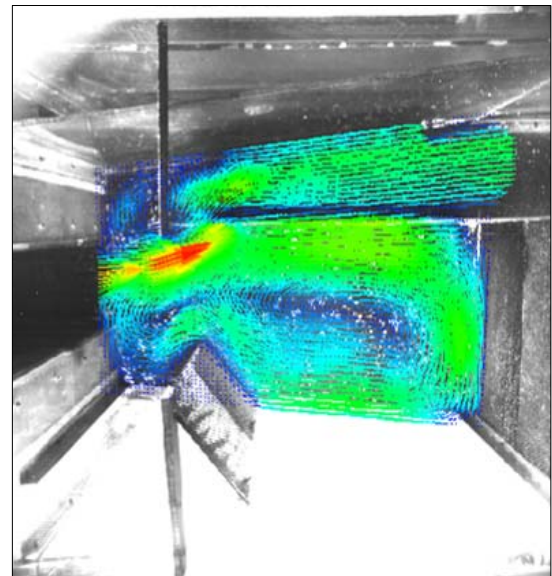
(b) R3
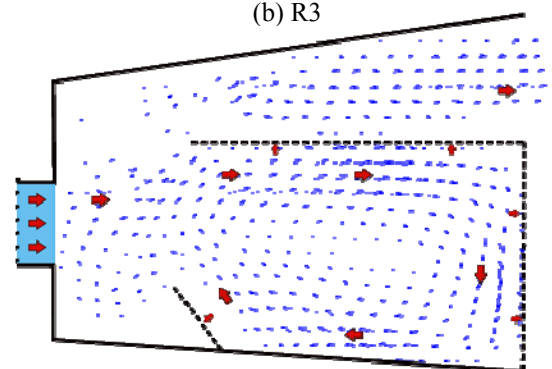
(c) R3.

Fig. 6. A single frame capture of the experimental flow for R3 (Table 2) with (a) particle seeding, (b) the vector plot from the data processed by the PIV software and (c) the improved vector plot using Matlab (version 2008b) for R3 dataset.

(zone 7). These areas may contribute to litter retention, and are identified as flow structures that can be optimized in GPT design.

Figs 7a and 9 generally show good comparisons between the LIC image and the CFD-generated flow domain for the R1 dataset. Most of the smaller flow features are visible unlike the previous ADV-measured flow which lacks spatial flow domain coverage (Madhani et al. 2009b). However, some irregularities or distorted flow patterns are noted behind the baffle (see zone 3 in Fig. 9a). This area is not clearly sighted by the camera and the reflective properties of the Perspex baffle would have influenced the low velocities captured. This behaviour is not shown for the R3 dataset since the internal structure of the GPT is coated with non-reflective paint. Also, small dark patches are occasionally observed in the LIC images (see corner behind baffle, R1 in Fig. 7a), which denote very low or zero velocities. Dark patches in the main flow which cause obvious discontinuities, are due to either a lack of seeding or to the fact that the overhead structures supporting the baffle and inner wall in the GPT obscure the camera sighting (Fig. 6a).

In Figs 7 and 8, the overall flow behaviour in the GPT for the given range flow regimes appears to show some similarities in the flow structures for all the experimental runs (see flow feature zone 1, Fig. 9a). The common flow feature displayed is an inner recirculation in the trap retention area.

For the experimental runs in which the inlet velocities are unaltered, slight differences are observed in the geometrical configuration of the inner recirculation

(see flow feature zone 1, Fig. 9a). These are attributed to the difference in water depth (see R1–R2, R3–R4 and R5–R6, Fig. 7).

Some distinct differences are noted in the geometrical characteristics of the inner recirculation zones with the 33% blocked screens for the higher flow regime (Fig. 7f). Here the momentum of the entry jet created vortex turbulence motion, resulting in water cascading vertically at the far corner of the retention area (see zone 7, upper right, Fig, 9a for location in Fig. 7f) as the water escaped through the screens.

Consequently, the inner recirculation zone is distorted and displaced to the opposite side. Concerning litter capture and retention, preliminary experiments show that a portion of litter rapidly accumulates in this area. However, the turbulence in this flow regime would tend to break up the softer stormwater pollutants.

Although the flow structure for the 68% blocked screen (R3 and R4 in Table 2) is similar to that of the 100% blocked screen, some differences are observed for the higher inlet flow regimes (6 L/s and 35 L/s). Unlike the case of a fully blocked GPT (Figs 8a and 8b), the jet entry was not strongly deflected into the bypass channel (Figs 8c-8f). Hence, the incoming litter is inclined to flow directly into the retention area of the GPT rather than escaping into the bypass channel. Such behaviour is observed with the preliminary litter experiments.

Overall the LIC images are found to be useful in describing the flow structures within the GPT and for better understanding litter capture and retention. The greater flow detail in the LIC images highlighted areas of abnormalities or

distortions arising from poor capture techniques caused by issues relating to lighting, particle seeding or data acquisition rates. Further work is underway to improve the colour scheme in order to explore the threshold of the low velocities due to reflected light near the boundaries, which are earmarked by normalized vector plots.

(a) R1   (b) R2
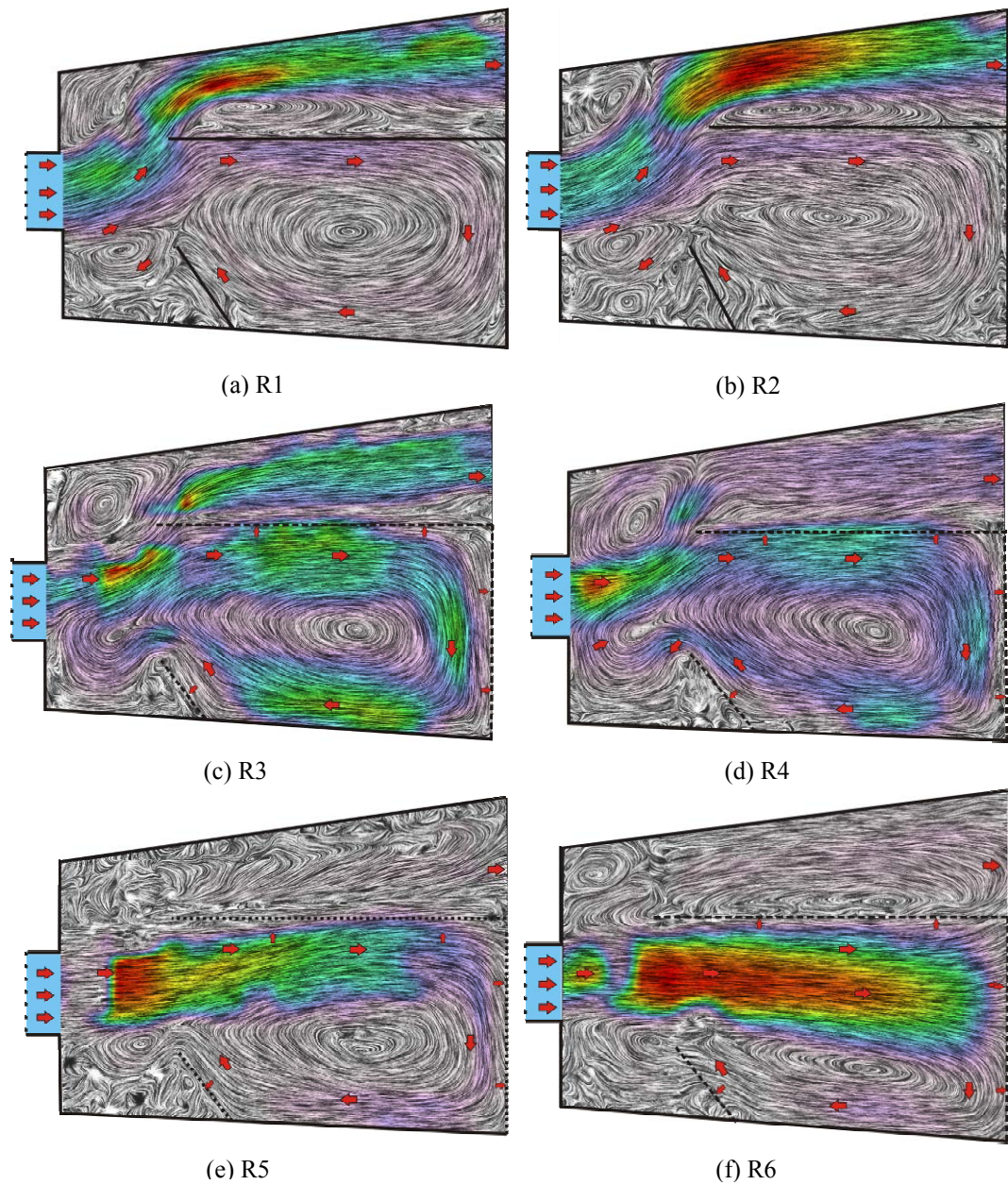
(c) R3   (d) R4

(e) R5   (f) R6

Fig. 7. Image based vector fields (a) R1, 100% blocked, water depth 0.1m; (b) R2, 100% blocked, water depth 0.3m; (c) R3, 68% blocked water depth 0.1m; (d) R4, 68% blocked water depth 0.3m; (e) R5, 33% blocked water depth 0.1m; (f) R6, 33% blocked water depth 0.3m; (See Table 2 for R1 to R6). Color map: red, yellow, green, blue and violet denotes high to low velocities respectively.

(a) R7
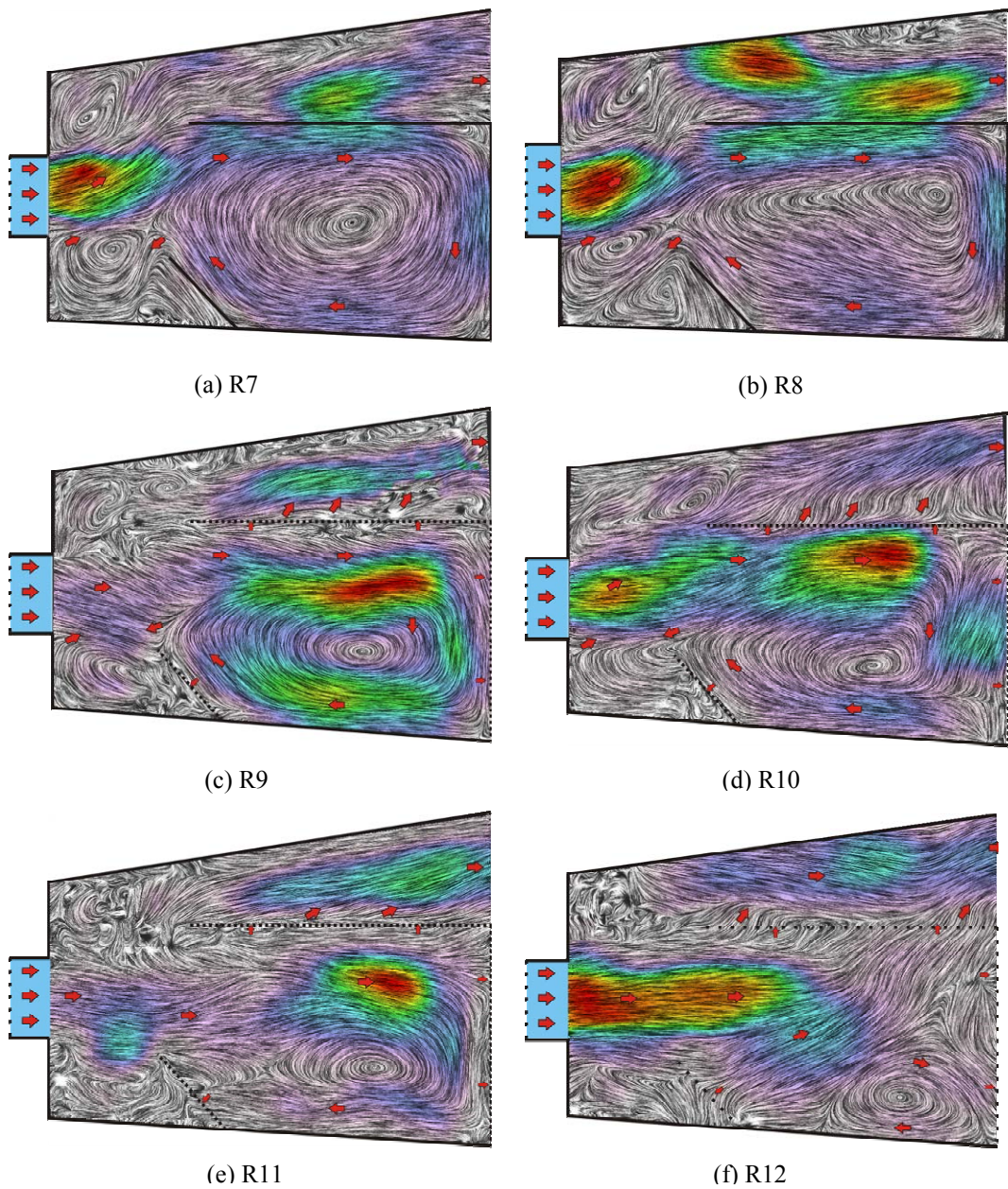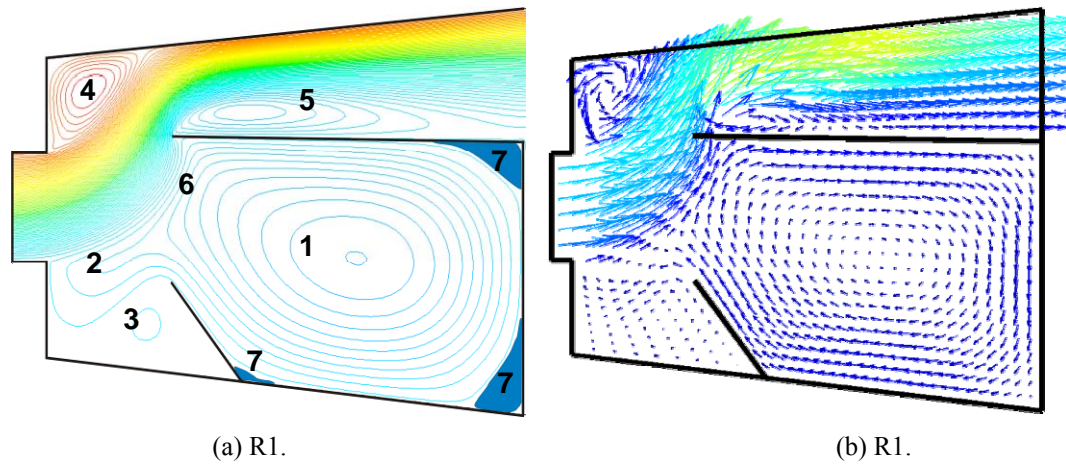
(b) R8

(c) R9

(d) R10

(e) R11

(f) R12

Fig. 8. Image based vector fields (a) R7, 100% blocked, water depth 0.1m; (b) R8, 100% blocked, water depth 0.3m; (c) R9, 68% blocked water depth 0.1m; (d) R10, 68% blocked water depth 0.3m; (e) R11, 33% blocked water depth 0.1m; (f) R12, 33% blocked water depth 0.3m; (See Table 2 for R8 to R12). Color map: red, yellow, green, blue and violet denotes high to low velocities respecitvely.

<center>(a) R1.   (b) R1.</center>

Feature zones
1, inner recirculation; 2, diverticulum; 3, 4, dead zone (secondary recirculation); 5, flow separation; 6, mixing; 7, low-velocity corner eddies.

Fig. 9. CFD global flow structures for run R1 in Table 2, in form of (a) streamlines and (b) vector plots. Source (Madhani et al. 2009)

Conclusion

A method is developed to capture and analyse several experimental flow regimes through a gross pollutant trap (GPT) with fully, partially and unblocked screens. The recorded fluid motions are visualized through an image-based, line integral convolution (LIC) algorithm and compared with conventional vector plots. The LIC method, a dense representation of streamlines, is found to be superior in highlighting flow features that are important for understanding litter capture and retention in the GPT. Overall, the results demonstrate the potential of the method in capturing and analysing flow in a GPT. This method was found to be very useful and applicable both in the laboratory and in the field, with little preparation and cost. For the application of field study, further investigation is required using organic particle seeding.

Detailed comparisons are made between the flow regimes, with favourable results compared with the previously defined CFD flow structure for fully blocked

screens. The LIC technique is also a useful tool in identifying abnormal flow structures in a GPT, which are often difficult to detect by conventional methods.

The experimental approach previously developed is also found to be useful in controlling a range of flow regimes in the GPT, which are necessary to perform experimental runs. Further work is underway to improve the technique of capturing the flow in the GPT and the method of producing LIC images to address issues with particle seeding and lighting thresholds.

Acknowledgements

References

1. Allison, R. A, & Chiew, F. H. S. (1995). Monitoring of stormwater pollution from various land uses in an urban catchment. The Second International Symposium on Urban Stormwater Management: Integrated Management of Urban Environments, Melbourne, Victoria, 11–13 July, vol. 2, pp. 511–516. Canberra: Institution of Engineers, Australia.

2. Allison, R. A., Walter, K. A., Marx, D., Lippner, G., & Churchwell, R. (2000). A method for monitoring and analysing litter in freeway runoff as part of the Caltrans Litter Management Pilot Study. In R. H. Hotchkiss and M. Glade (Eds), Joint Conference on Water Resources Engineering and Water Resource Planning and Management, Minneapolis, Minnesota, USA,

July 30–August 2, vol. 104, pp. 81. Virginia: American Society of Civil Engineers (ASCE).

3. Brisbane City Council (2004). Stormwater quality improvement devices (SQIDs) monitoring program summary. Draft report prepared by Water and Environment, City Design for Waterways Program. Queensland, Australia: Brisbane City Council.

4. Borchardt D. and Sperling F. (1997). Urban stormwater discharges: ecological effects on receiving waters and consequences for technical measures. *Water Science and Technology*, 36(8-9), 173–178.

5. Cabral, B., & Leedom, C. (1993). Imaging vector fields using line integral convolution. In M. Whitton, (Ed.), The 20th Annual Conference on Computer Graphics and Interactive Techniques (SIGGRAPH '93), Anaheim, California, August 1–6, vol. N/A, pp. 263–270. New York: Association for Computing Machinery (ACM) Press.

6. Chrispijn, J. (2004). Assessing different at-source stormwater treatment devices in Hobart: Sullivans Cove and Brooker Highway performance trials. Stormwater Industry Association (SIA) bulletin, issue 117. http://www.stormwater.asn.au/tas/Enviro04Paper-Chrispijn.pdf. Accessed 6 April 2009.

7. Cordery, I. (2005). Field performance of a vortex type gross pollutant trap. Australian Journal of Water Resources, 9(1), 49–54.

8. Greenway, M., Muth, N. L., & Jenkins, G. (2002). Monitoring spatial and temporal changes in stormwater quality through a series of treatment trains: a case study, Golden Pond, Brisbane, Australia. In E. W. Stricker & W. C. Huber (Eds), The 9th International Conference on Urban Drainage (9ICUD),

Portland, Oregon, USA, Sept 8–13, vol. 112, pp. 52. Virginia: American Society of Civil Engineers (ASCE).

9. Harwood R. (2002). CSO modelling strategies using computational fluid dynamics. In E. W. Stricker & W. C. Huber (Eds), The 9th International Conference on Urban Drainage (9ICUD), Portland, Oregon, USA, Sept 8–13, vol. 112, pp. 8. Virginia: American Society of Civil Engineers (ASCE). http://www.hydrointernational.biz/irl/other/information_library.php. Accessed 6 April 2009.

10. Hossain, M. Z., Hirahara, H., Nonomura, Y., & Kawahashi, M. (2007). The wake structure in a 2D grid installation of the horizontal axis micro wind turbines. *Renewable Energy*, 32(13), 2247-2267.

11. IDT (2005a). X Stream[TM] Vision cross-platform user manual for high-speed CMOS digital camera (software version 1.13). Integrated Design Tools Inc. http://www.idtvision.com. Accessed 6 April 2009.

12. IDT (2005b). proVision-XS user manual for particle image velocimetry (software version 3.08). Integrated Design Tools Inc. http://www.idtvision.com. Accessed 6 April 2009.

13. Kandlikar, S. G., Lu, Z., Domigan, W. E., White, A. D., & Benedict, M. W. (2009). Measurement of flow maldistribution in parallel channels and its application to ex-situ and in-situ experiments in PEMFC water management studies. *International Journal of Heat and Mass Transfer*, 52(7-8), 1741-1752.

14. Kao, D. L., & Shen, H-W. (1998). Numerical surface flow visualization, NAS Technical Report, NAS-98-001, NASA. http://www.nas.nasa.gov/-News/Techreports/1998/PDF/nas-98-001.pdf. Accessed 20 March 2009.

15. Lewis, J. (2002). Effectiveness of stormwater litter traps for syringe and litter removal. Cooperative Research Centre (CRC) for Catchment Hydrology. Report prepared for Melbourne Water Corporation, Melbourne Australia. http://www.clearwater.asn.au/resources/325_1.pdf. Accessed 6 April 2009.

16. Li, C.-T., Chang, K.-C., & Wang, M.-R. (2009). PIV measurements of turbulent flow in planar mixing layer. *Experimental Thermal and Fluid Science*, 33(3), 527-537.

17. Lippner, G., & Moeller, G. (2000). Study quantifies broom sweeper litter pickup ability. American Sweeper Magazine, 8(1). http://www.owp.csus.edu/research/papers/. Accessed 6 April 2009.

18. Madhani, J. T., Dawes, L. A., & Brown, R. J. (2009a). A perspective on littering attitudes in Australia. *The Environmental Engineer*: Journal of the Society for Sustainability and Environmental Engineering, vol. 9(4), pp. 13. Canberra: The institution of Engineers, Australia.

19. Madhani, J. T., Kelson, N. A., & Brown, R. J. (2009b). An experimental and theoretical investigation of flow in a gross pollutant trap. *Water Science and Technology*, 59(6), 1171–1127.

20. Nielsen, J. S., & Carleton, M. G. (1989). A study of trash and trash interception devices on the Cooks River catchment, Sydney. Proceedings of the Australian Water and Wastewater Association 13th Federal Convention, Canberra, March, vol. n/a, pp. 126–129. Canberra: Institution of Engineers, Australia.

21. Quasebarth, T., Schroeder, D., Chappell, R., Churchwell, R., & Lippner, G. (2001). An investigation of factors influencing solids transport and deposition into highway drain inlets. In D. Phelps & G. Sehlke (Eds), Bridging the gap: meeting the world's water and resources challenges. World Water and

22. Renka. R. J., & Cline, A. K. (1992). Scattered data fitting using a constrained Delaunay triangulation. International *Association for Mathematics and Computers in Simulation (IMACS) Transactions on Scientific Computing*: AI, Expert Systems, and Symbolic Computation, North Holland, June, vol. 3, pp. 208–214.

23. Renka, R. J. (1996a). Algorithm 751: TRIPACK: a constrained two-dimensional Delaunay triangulation package. *Association for Computing Machinery (ACM) Transactions on Mathematical Software (TOMS)*, 22(1), 1-8. New York: ACM Press.

24. Renka, R. J. (1996b). Algorithm 752: SRFPACK: software for scattered data fitting with a constrained surface under tension. *Association for Computing Machinery (ACM) Transactions on Mathematical Software (TOMS)*, 22(1), 9–17. New York: Association for Computing Machinery (ACM) Press.

25. Rushton B., England G. & Smith D. (2007). Proposed Guidelines for Monitoring Stormwater Gross Solids. In K. C. Kabbes (Ed), World Environmental and Water Resources Congress 2007, Tampa, Florida, USA, May 15-19, vol. 243, pp. 58. Virginia: American Society of Civil Engineers (ASCE).

26. Stalling, D., & Hege, H.-C. (1995). Fast and resolution independent line integral convolution. In S. G. Mair & R. Cook (Eds), The 22nd Annual Conference on Computer Graphics and Interactive Techniques (SIGGRAPH '95), Los Angeles, California, August 6–11, vol. n/a, pp. 249–256. New York: Association for Computing Machinery (ACM) Press. http://portal.acm.org/citation.cfm?id=218448. Accessed 6 April 2009.

27. Stovin, V. R., Saul, A. J., Drinkwater, A., & Clifforde, I. (1999). Field testing CFD-based predictions of storage chamber gross solid separation efficiency. *Water Science and Technology*, 39(9), 161–168.

28. Telea, A. C., & van Wijk, J. J. (1999). Simplified representation of vector fields. In A. Telea & J. J. van Wijk (Eds), Proceedings of the 10th IEEE Visualization Conference 1999 (VIS '99), San Francisco, California, October 24–29, vol. n/a, pp. 35–42. http://ieeexplore.ieee.org/stamp/stamp.jsp?tp=-&ar-number=809865. Accessed 6 April 2009.

29. Thackston, E. L., Shields, D. F., & Schroeder P. R. (1987). Residence time distributions of shallow basins. *Journal of Environmental Engineering*, 113(6), 1319–1332.

30. Turk, G., & Banks, D. (1996). Image-guided streamline placement. In J. Fujii (Ed.), The 23rd Annual Conference on Computer Graphics and Interactive Techniques (SIGGRAPH '96), New Orleans, Los Angeles, August 4–9, vol. n/a, pp. 453–460. New York: Association for Computing Machinery (ACM) Press.

31. Van Drie, R. (2002). Development of a pollutant load algorithm (for Sydney Australia). In E. W. Stricker & W. C. Huber (Eds), The 9th international conference on urban drainage (9ICUD), Portland, USA, Sept 8–13, vol. 112, pp. 207. Virginia: American Society of Civil Engineers (ASCE).